Materials Today Advances 12 (2021) 100194

Contents lists available at ScienceDirect

Materials Today Advances

journal homepage: www.journals.elsevier.com/materials-today-advances/

# Controlling macroscale cell alignment in self-organized cell sheets by tuning the microstructure of adhesion-limiting micromesh scaffolds

Kennedy Omondi Okeyo [a, b, *], Yoshikiyo Kibe [b], Taiji Adachi [a, b]

[a] Institute for Frontier Life and Medical Sciences, Kyoto University, 53 Shogoin Kawahara-cho, Sakyo-ku, Kyoto, 606-8507, Japan
[b] Division of Systemic Life Science, Graduate School of Biostudies, Kyoto University, Yoshida-Konoecho, Sakyo-ku, Kyoto, 606-8501, Japan

ARTICLE INFO

*Article history:*
Received 26 September 2021
Received in revised form
27 November 2021
Accepted 28 November 2021
Available online 2 December 2021

*Keywords:*
Regenerative medicine
Cell sheets
Cell alignment
Cell adhesion
Scaffold microstructure
Geometry sensing

ABSTRACT

In vivo tissues, including the cardiac, skeletal muscles, tendon and ligaments display characteristic alignment property which is important for their mechanical property and functionality. Mimicking this alignment property is critical to the realization of physiologically relevant cell sheets for potential application in the regeneration of aligned in vivo tissues. In this study, we aimed to achieve fabrication of aligned cell sheets by harnessing the ability of cells to sense and respond to geometrical cues in their adhesion microenvironment. We demonstrate that macroscale cell alignment in cell sheets formed by C2C12 cells, a mouse myoblast cell line, on adhesion limiting microstructured mesh scaffolds depends on the shape of the scaffold microstructure. Specifically, while square meshes produced cell sheets with random orientation, diamond meshes yielded anisotropic cell sheets with cells aligned uniaxially along the major axis of the diamond shape. Moreover, alignment intensity was found to increase concomitantly with the acuteness of the diamond shape, illustrating alignment dependency on mesh shape anisotropy. Remarkably, myotubes derived from aligned C2C12 cells also displayed a similar alignment trend, demonstrating the robustness of our approach. Taken together, the present study demonstrates the potential to control macroscale cell alignment in self-organized cell sheets by tuning the shape of the scaffold microstructure. Thus, insights from this study could be relevant to the design of instructive scaffolds for fabricating aligned cell sheets for potential application not only in regenerative medicine, but also in developing muscle constructs for toxicity assays.



## 1. Introduction

Cell sheets are tissue-engineered cellular constructs in the form of intact confluent cell layers which are increasingly attracting attention for their potential application in regenerative medicine [1,2]. Indeed, past and ongoing animal and clinical studies have demonstrated the potential application of cell sheets in regenerative medicine targeting different tissues/organs, including the cornea [3,4], articular cartilage [5] and myocardial tissues [6,7]. Thus, cell sheets are promising biomaterials for regenerative medicine.

In vivo tissues such as the cardiac and skeletal muscles, tendons, and ligaments display characteristic alignment which is important for their mechanical property and functionality. Hence, for cell sheet application in the regeneration of these tissues, controlling macroscale (global) cell alignment in cell sheets is highly necessary. To this end, attempts have been made to fabricate anisotropic (aligned) cell sheets using temperature-responsive polymers [8–10] integrated with the conventional techniques for controlling cell alignment such as micropatterning and micro/nano grooves [11–14]. For instance, Takahashi et al. [15,16] demonstrated fabrication of aligned cell sheets of human skeletal muscle myoblasts on a micropatterned thermoresponsive surface. In addition, cell alignment has been induced in cell sheets by application of a mechanical stretch [17,18]. However, despite these attempts, controlling cell alignment in cell sheets remains challenging partly due to the low mechanical strength and fragility of these biomaterials. Thus, alternative approaches are highly desirable to achieve fabrication of anisotropic cell sheets while maintaining the cell-cell connection from which cell sheets derive their mechanical strength.

Traditionally, scaffold-based approach has been applied in tissue engineering majorly because scaffolds support initial cell growth

* Corresponding author. Institute for Frontier Life and Medical Sciences, Kyoto University, 53 Shogoin Kawahara-cho, Sakyo-ku, Kyoto, 606-8507, Japan.
*E-mail address:* okeyo@infront.kyoto-u.ac.jp (K.O. Okeyo).

https://doi.org/10.1016/j.mtadv.2021.100194

and direct tissue formation, and confer mechanical strength to the fragile tissues, allowing for better integration when implanted in vivo. For cell sheets, which are themselves 2D cellular constructs, 2D culture systems are more compatible and offers a higher degree of controllability. Indeed, 2D scaffolds and culture systems remain relevant in tissue engineering [2,19], especially because they are generally low cost, easy to image, relatively easy to design to control specific cell behaviors, such as differentiation and alignment. Taking the scaffold-based approach, we have developed a cell sheet fabrication technique (micromesh technique) which employs 2D microstructured mesh substrates (micromesh scaffolds) with characteristically large mesh size (characteristic aperture length >100 μm) and fine mesh lines (width ~5 μm) [20]. By setting the scaffolds suspended in the culture medium for cell seeding and culture, cells on the mesh grow under the condition of highly restricted cell-substrate interaction. In the previous studies, we have demonstrated that this adhesion restriction entices cells to self-organize naturally into cell sheets while relying majorly on cell-cell adhesion [20–22]. Moreover, in a past preliminary study, we reported that mesenchymal cells could exhibit alignment under the micromesh culture [23], but the mechanism remained to be clarified.

In this study, we sought to harness the ability of cells to sense and respond to geometrical cues in their adhesion microenvironment to achieve fabrication of aligned cell sheets using the micromesh technique [20]. We focused on elucidating the influence of scaffold microstructure, in particular mesh shape, on macroscale cell alignment in cell sheets generated by this technique. For this purpose, we fabricated microstructured 2D scaffolds with various mesh shapes, and examined the emergence of alignment during the self-organized cell sheet formation by C2C12 cells cultured on the micromesh scaffolds. For simplicity, we focused on the diamond shape and fabricated micromesh scaffolds with mesh shapes ranging from a square shape to an acute diamond shape by designing photomasks with diamond patterns of varying the acute vertex angle (henceforth referred to as shape angle and denoted by $\psi$).

Our results show that while scaffolds with square meshes (shape angle $\psi = 90^\circ$) produced cell sheets with random orientation, those with diamond shapes ($\psi < 90^\circ$) yielded cell sheets exhibiting uniaxial cell alignment along the major axis of the diamond shapes. Global cell alignment emerged in response to the microscale mesh shape, with alignment intensity increasing concomitantly with acuteness of the diamond shapes tested ($\psi = 90^\circ$, $70^\circ$, $50^\circ$, $30^\circ$). In addition, we also show that myotubes derived from aligned C2C12 cells on the diamond meshes could retain similar alignment, illustrating robustness of our alignment approach. Thus, we demonstrate the possibility to achieve macroscale alignment control in self-organized cell sheets simply by tuning the shape of the scaffold microstructure. The findings of this study will have important implications for the design of instructive scaffolds meant for fabricating aligned cell sheets for potential application in regenerative medicine.

## 2. Materials and methods

### 2.1. Fabrication of microstructured two-dimensional micromesh scaffolds

Microstructured 2D micromesh scaffolds used in this study were fabricated by standard photolithography using SU-8 (epoxy-based negative photoresist), as reported previously [20,21]. Briefly, photomask blanks were laser-patterned using a Laser Pattern Generator (Heiderberg Instruments, DWL2000, Germany) and processed to generate photomasks with micromesh patterns of different shape angles. Then, the photomasks were used to pattern SU-8-2 layers (thickness ~2 μm) spin-coated on 4-inch silicon wafers to generate micromesh scaffolds as follows. First, SU-8-2 was spin-coated at 2000 rpm on a silicon wafer precoated with a gelatin sacrificial layer, then exposed to UV light via the patterned photomasks using a contact mask aligner (Mikasa, Japan). After development in SU-8 developer (1-Methoxy-2-propanol acetate, Microchem, Japan) with agitation for 3 min and rinsing in isopropanol for 1 min, the SU-8 patterns on wafer were laminated with rigid adhesive tapes (Kapton tape, Nitto, USA) punched with a center hole ($\phi = 4$ mm) to provide reinforcement after detachment and for handling during cell culture. To ensure adhesion restriction by avoiding cell interaction with the dish bottom during culture, the 2D micromesh scaffolds were setup in a raised position at a height of 0.5 mm from the dish bottom using silicone rubber spacers. To facilitate cell attachment, fibronectin coating was performed by placing a 100 μL droplet of 100 μg/mL fibronectin solution (Wako, Japan) in 1 × PBS (phosphate buffered saline) atop the suspended scaffolds, followed by incubation for more than 60 min inside an incubator.

To examine the effect of microstructure shape on cell alignment, we fabricated and analyzed alignment on micromesh scaffolds with shape angles ranging from $\psi = 90^\circ$–$30^\circ$; with $\psi = 90^\circ$ denoting a square shape, and $\psi = 30^\circ$ denoting the most acute diamond shape. We performed most analysis using scaffolds with an aperture size L = 200 μm (taken as the length of the minor diagonal), and additional validation experiments with L = 100 μm.

### 2.2. Cell seeding and culture on the micromesh scaffolds

C2C12 cells, a mouse myoblasts cell line, were mainly used in this study. Unlabeled C2C12 cells were sourced from ATCC, and GFP-tagged C2C12 cells [24] were sourced from RIKEN cell bank (Japan). In a separate preliminary experiment, we tested alignment using TIG-120 cells (Normal diploid fibroblast from human skin, #JCRB054, RIKEN cell bank, Japan). These cells were expanded on polystyrene dishes in high glucose Dulbecco's Modified Eagle Medium (DMEM) containing 10% FBS (fetal bovine serum, Gibco) and 1% antibiotic-antimycotic (Sigma-Aldrich, Germany).

The 2D micromesh scaffolds were setup and seeded with cells essentially as reported previously [20]. Briefly, dish-cultured cells at 70–80% confluency were dissociated with 0.25% trypsin, resuspended in a fresh culture medium (DMEM+10% FBS), and then seeded on the fibronectin-coated micromesh scaffolds by placing a 100 μL droplet containing approximately $10^5$ cells directly atop the suspended scaffolds (effective mesh area 12.6 $mm^2$). Then, the cell-seeded scaffolds were transferred to an incubator and left unperturbed to allow for cell attachment. Fresh medium was added after 12 h, and culture was continued with medium exchange after every 3 days until cell sheet formation. For cell tracking and alignment analysis, unlabeled and GFP-tagged C2C12 (GFP-C2C12) were mixed at a ratio of 20:1 during seeding on the micromesh scaffolds.

### 2.3. Live cell imaging and F-actin labeling

To capture cell dynamics during the self-organized cell sheet formation on the micromesh scaffolds, we performed timelapse imaging using an all-in-one fluorescence microscope (Keyence, Japan) equipped with an onstage incubator with an inline gas mixture (Tokai Hit, Japan) which supplied 5% $CO_2$ during the onstage culture. Imaging was performed right from day 1 of cell

seeding on the scaffolds to day 7 when alignment was fully formed, using 4 × , 10 × and 20 × phase contrast objective lenses, and acquisition interval of 20 min.

To visualize filamentous actin (F-actin), cells were stained by fixing with 4% paraformaldehyde for 15 min, followed by permeabilization with 0.5% triton-100 for 15 min. Alexa Fluor 488 Phalloidin (Invitrogen, USA) at a 1:400 dilution and DAPI (4′,6-diamidino-2-phenylindole) at a1:1000 dilution in 1 × PBS were used to stain F-actin and nuclei, respectively.

### 2.4. Analysis of cell alignment

Cell alignment was analyzed based on the acquired images of GFP-C2C12 at day 7 of micromesh culture. The analysis was performed using "Orientation J", a plugin available publicly on Image J (NIH, USA) [25], using the following parameters: grid size; 30 pixels, local window $\sigma = 2$ pixels, gradient; cubic spline, vector scale; 80%.

Alignment intensity, a measure of how well cells align in a particular direction θ, was analyzed by computing the sum of vector elements with orientation falling within $\theta \pm 15^{\circ}$ range, and then expressed as a percentage of the total sum of all vector elements for the entire image analyzed. Orientation angle, θ, was taken with respect to the horizontal direction ($\theta = 0^{\circ}$ direction), which corresponded to the major axis of a diamond mesh. Alignment graphs were presented as mean ± sd (standard deviation). Statistical significance was determined using student's t-test ($p < 0.05$) for each experimental condition with a sample number of $N = 5$ or more.

## 3. Results

### 3.1. Self-organized cell sheet formation on adhesion-limiting micromesh scaffolds

In this study, we fabricated microstructured micromesh scaffolds and used them to induce cell sheet formation as reported previously [20]. To monitor the mesh closure process and the resulting cell sheet formation, we performed timelapse microscopy for a co-culture of unlabeled C2C12 and GFP-expressing C2C12 (GFP-C2C12) mixed before seeding at a ratio of 20:1, respectively, on scaffolds with square (shape angle $\psi = 90^{\circ}$) and diamond meshes ($\psi = 70^{\circ}$), as illustrated in Fig. 1A and Fig. S1.

Despite the high porosity (>90%) of the micromesh scaffolds, cells could successfully attach on the narrow mesh lines and could be seen elongating along them by Day 1 (Fig. 1B and C, Day 1). Cells adhered on the mesh lines began to proliferate and self-organize

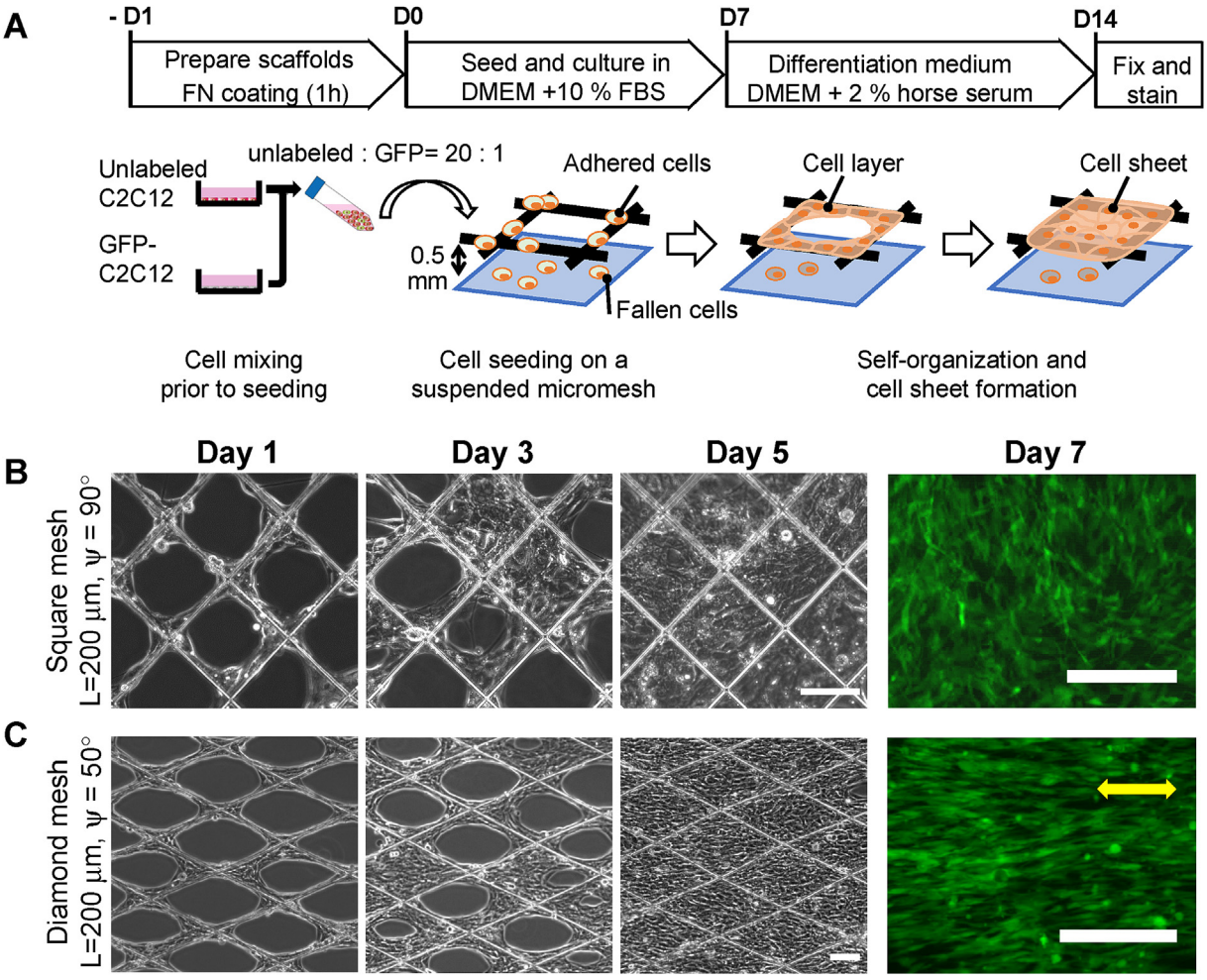


**Fig. 1.** Self-organization and cell sheet formation on adhesion-limiting 2D micromesh scaffolds. A: Cell culture scheme and a schematic illustrating the self-organization processes leading to cell sheet formation on the micromesh scaffolds. The scaffolds were set suspended at a height of 0.5 mm above the dish bottom. B–C: Timelapse images depicting the self-organization of C2C12 cells on a square mesh versus a diamond mesh, and the resulting cell orientation in the cell sheets formed on the two micromesh scaffolds (right panel). The fluorescent images on the right panel of B and C are for GFP-C2C12 cells at day 7. The yellow arrow in C indicates alignment direction. Scale bar: 100 μm.

into a duck-foot-like cell layer around each mesh (Fig. 1, Day1). The mesh filling process continued as each mesh became covered with a layer of cells expanding from the mesh lines, and, by Day 3, partially and fully covered meshes could be observed (Fig. 1B and C, Day 3). Timelapse microscopy revealed rapid cell migration along the mesh lines, with cells traversing several meshes at the initial stages of self-organization, but cell movement declined and became more localized with increasing cell density at the later stages (Movie S1). By Day 5, nearly all meshes had been covered, yielding a uniform cell layer over the entire micromesh scaffold (Fig. 1B and C, Day 5).The time to cell sheet formation was nearly the same for both the square and diamond meshes. It should be noted that mesh size was a key factor influencing the retention of cells on the scaffolds during seeding, and therefore determined the speed of cell sheet formation. For the scaffolds with mesh size L = 200 μm (aperture length), porosity was approximately 97.6%. This implies that nearly this percentage of cells would fall off to the dish bottom during seeding. Given that we seeded 500,000 cells on the micromesh scaffold (ϕ = 4 mm), we estimated that approximately 12,000 cells would remain on the mesh lines to proliferate, undergo self-organization, and eventually form a cell sheet. Mesh size (area) as factor of cell siz, and porosity are summarized in Tables S1 and S2, respectively.Supplementary Movie 1: Timelapse movie showing the dynamics of GFP-expressing C2C12 cells during self-organized cell sheet formation on a diamond mesh.

Supplementary data related to this article can be found at https://doi.org/10.1016/j.mtadv.2021.100194.

Another notable observation during the cell sheet formation process was the striking difference in the shape of the leading front of the expanding cell layer during the closure process. While the leading front was visibly circular in the case of the square meshes (Fig. 1B, Day 1, 2), this was largely oval and elongated in the major axis in the case of diamond meshes (Fig. 1C, Day 1, 2). In the latter case, cells migrating along the leading front of the enclosing cell layer exhibited remarkable stretching along the major axis of the diamond meshes (yellow arrows in Fig. S2, Movie S1), in a manner suggestion mechanical edge tension analogous to that reported for wound closure [26].

By Day 7, we could notice a clear difference in cell orientation between the two mesh shapes (Fig. 1B and C, Day 7). While cell sheets on square meshes exhibited random cell orientation (Fig. 1B), those on diamond meshes displayed uniaxial cell alignment, both at the micro and global scale, with cells aligned distinctively along the major axis of the diamond meshes (Fig. 1C). In the latter case, alignment began to emerge around the time of complete mesh filling at Day 5, and became increasingly pronounced as compaction continued due to increasing cell density on the formed cell sheets (Fig. 1C, Day 7). Nevertheless, as confirmed in a separate experiment (Fig. S2B), alignment could still emerge even at extremely low cell density on the diamond micromesh scaffolds (Fig. S2B), with cells exhibiting a tendency to orient along the major shape axis well before the mesh apertures were completely covered. Consistent with the results in Fig. 1C, Day 7, alignment in this case appeared more pronounced after complete cell sheet formation, suggesting that alignment strength increased with increasing cell density on the scaffolds. Importantly, the fact that only diamond meshes, but not square meshes, could generate aligned cell sheets with global alignment (Fig. 2) provided a hint

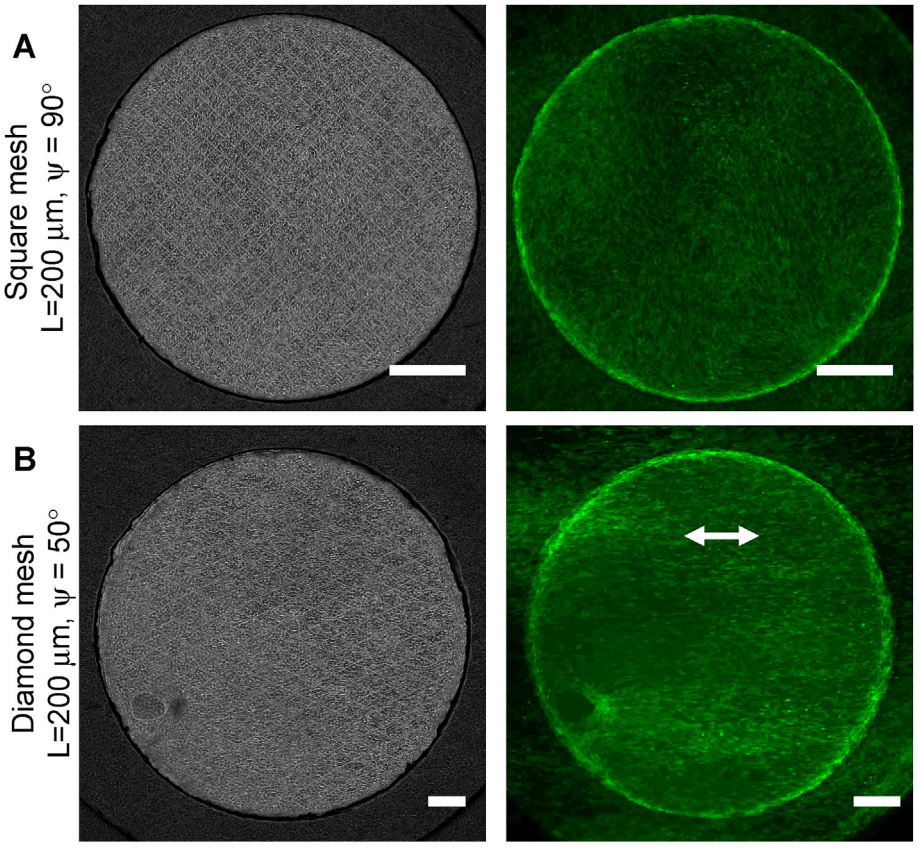


**Fig. 2.** Wide field view of cell alignment in cell sheets generated on the 2D micromesh scaffolds. A: Cell sheet formed on a square mesh scaffold exhibiting a random cell alignment. B: Aligned cell sheet formed on a diamond mesh scaffold. Phase contrast images on the left panel show both unlabeled and GFP-C2C12 cells, while the fluorescent images on the right panel show alignment of GFP-C2C12. White arrow indicates alignment direction. Scale bar is 500 μm.

that the scaffold microstructure may influence cell alignment in cell sheets. Prompted by this result, we sought to determine the effect of microscale mesh shape on global cell alignment by assessing cell alignment in response to varying mesh shape angle, ψ (Fig. 2A).

### 3.2. Relationship between alignment intensity and mesh shape anisotropy

To further establish the relationship between cell alignment and microscale mesh shape, we fabricated and tested scaffolds with varying mesh shapes; ranging from a regular square ($\psi = 90^\circ$) to an acute diamond shape ($\psi = 50^\circ$), while keeping the characteristic aperture length L constant (L = 200 μm). It should be noted that changing the mesh shape angle resulted in a slight change in mesh size, as illustrated in Fig. S1 and Table S1. Quantitative analysis of cell alignment corresponding to each shape angle was performed based on the images of GFP-C2C12 at day 7 (Fig. 1B and C, right). Alignment intensity was quantified along a given angular direction specified with respect to the $\theta = 0^\circ$ direction, which was set corresponding to the major axis of the diamond shape, as depicted in Fig. 3A. Alignment distribution graphs for mesh scaffolds with shape angles $\psi = 90^\circ$, $70^\circ$ and $50^\circ$ are compared in Fig. 3B. For square meshes (shape angle, $\psi = 90^\circ$), we found that alignment intensity was uniformly distributed, a clear indication of a random orientation. In contrast, for diamond meshes ($\psi = 70^\circ$ and $50^\circ$), alignment was predominantly within $-30^\circ \leq \theta \leq 30^\circ$ range with respect to the major shape axis ($\theta = 0^\circ$), which implies uniaxial alignment in the $\theta = 0^\circ$ direction (Fig. 3B).

Remarkably, alignment intensity in the $\theta = 0^\circ$ direction increased markedly with decreasing shape angle ψ (Fig. 3C), an indication of sensitivity to the acuteness of the diamond shape (shape anisotropy). Indeed, compared with alignment intensity of about 17% for square meshes ($\psi = 90^\circ$), acute diamond meshes ($\psi = 50^\circ$) yielded an alignment intensity of over 80%, indicating that mesh shape exerts considerable influence on alignment. Consistently, a confirmatory experiment performed using diamond meshes with a characteristic aperture length of L = 100 μm produced similar results (Fig. S3). In this case, alignment intensity for a diamond mesh with $\psi = 30^\circ$ was found to be significantly higher than for $\psi = 70^\circ$ (Fig. S3). Additional validation experiments performed using TIG-120 cells (normal diploid fibroblast from human skin) further confirmed alignment dependency on mesh shape anisotropy, with cells showing uniaxial alignment on scaffolds with diamond meshes and 30°-triangular meshes but not on square meshes and 50°-triangular meshes (Fig. S4). Collectively, these results demonstrated that cell alignment in the self-organized cell sheets emerged in response to mesh shape anisotropy.

Since the focus of this study was to determine the effect of mesh shape (pore shape) on alignment, we chose to examine alignment in response to mesh shape changes while keeping the aperture length L constant (L = 200 μm or L = 100 μm). Nevertheless, it should be mentioned that mesh size was a key factor influencing

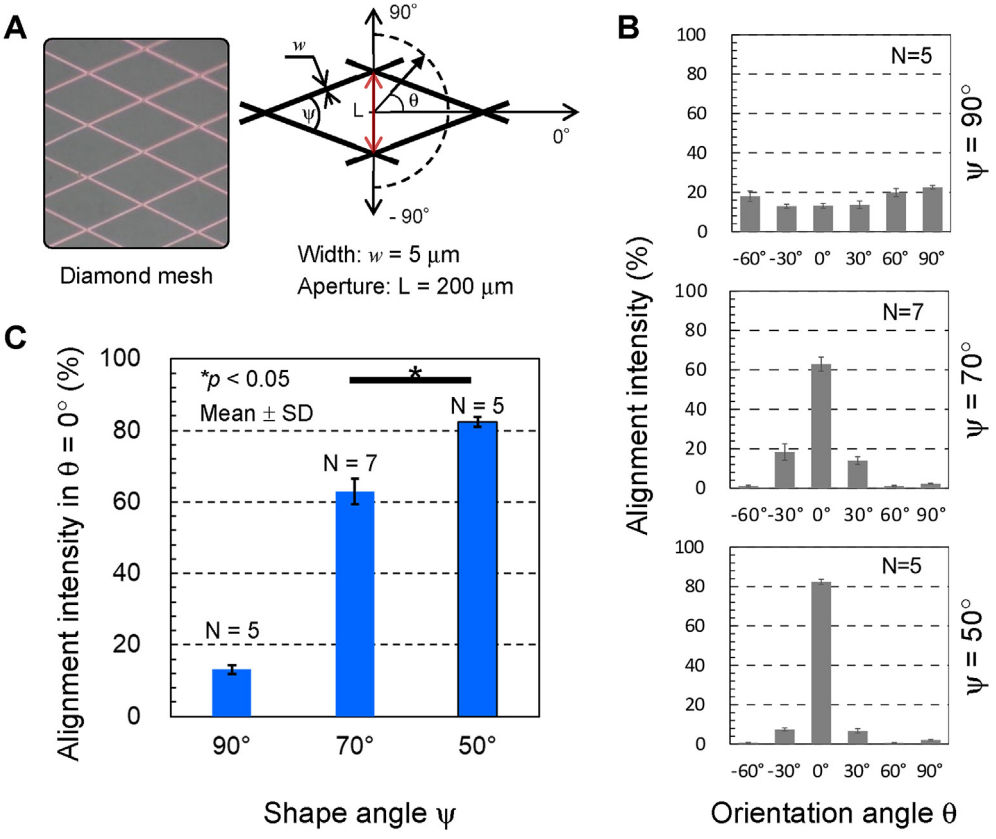


**Fig. 3.** Quantitative analysis of cell alignment with respect to mesh shape. A: Image of a diamond mesh and a schematic defining shape dimensions and symbols. B: Distribution of alignment intensity with orientation angle for the different mesh shapes investigated (represented by shape angle ψ). C: Relationship between alignment intensity and mesh shape. Orientation intensity increased significantly with decreasing shape angle.

retention of cells on the scaffolds during seeding, and therefore determined the speed of cell sheet formation. For instance, for large size meshes (L ≥ 200 μm), the duration to cell sheet formation took longer since fewer cells would remain on the mesh surface compared with small size meshes (L ≤ 100 μm). In separate other studies (unpublished data), we have tested different mesh sizes ranging from L = 30 μm–300 μm and found that for extremely large mesh size, for instance L = 300 μm, the duration to cell sheet formation was too long (over 14 days) and the emerging alignment tended to be weaker compared with mesh sizes below L = 200 μm. Conversely, mesh sizes below 100 μm would yield cell sheets rapidly (in less than 3 days, but with disturbed alignment. Hence, a mesh size range of L = 100–200 μm was chosen as the optimal range for evaluating alignment response in relation to mesh shape.

Since the actin cytoskeleton provides the mechanical framework to support cell bridging during mesh closure and cell sheet formation, we next sought to determine F-actin alignment in the self-organized cell sheets. Staining results revealed a uniformly spread F-actin meshwork, with actin fibers traversing the mesh apertures (Fig. 4). Whereas F-actin fibers in cell sheets on square meshes ($\psi = 90^\circ$) appeared disorganized and randomly oriented (Fig. 4A), consistent with the random cell orientation on these scaffolds (Fig. 1B and C, Day 7), the diamond meshes ($\psi = 70^\circ$ and $50^\circ$) exhibited uniaxially aligned F-actin fibers, with alignment conforming to the major shape axis (Fig. 4C and D).

Taken together, these results confirmed the dependency of global cell alignment on microscale mesh shape, with alignment showing sensitivity to mesh shape anisotropy. This is consistent with previous studies demonstrating the influence of anisotropic topographical cues on cell alignment [27,28].

### 3.3. Myotubes derived from aligned C2C12 cells exhibit similar alignment trend

To verify if alignment could be maintained even after myotube formation, we switched to a differentiation medium consisting of DMEM supplemented with 1% horse serum from Day 7. Myotubes started to appear after 3 days of differentiation induction, and continued to increase in number as well as length with time. Noticeably long myotubes could be observed after 6 days of differentiation induction (Fig. 5A, $\psi = 70^\circ$).

As shown in Fig. 5B, scaffolds with square meshes generated randomly oriented myotubes, consistent with the orientation of C2C12 on this mesh pattern. In contrast, myotubes on scaffolds with diamond meshes appeared to be more aligned (Fig. 5A, C), and were visibly elongated along the major axis of the diamond shape, which conformed to the orientation of C2C12 cells prior to differentiation induction. This would suggest that myotubes formed from aligned C2C12 are able to retain the alignment property of their precursors. Immunostaining for α-actinin (Fig. 5B and C), however, did not reveal any noticeable sarcomere formation, neither did we observe contraction, implying that the myotubes derived on mesh were still

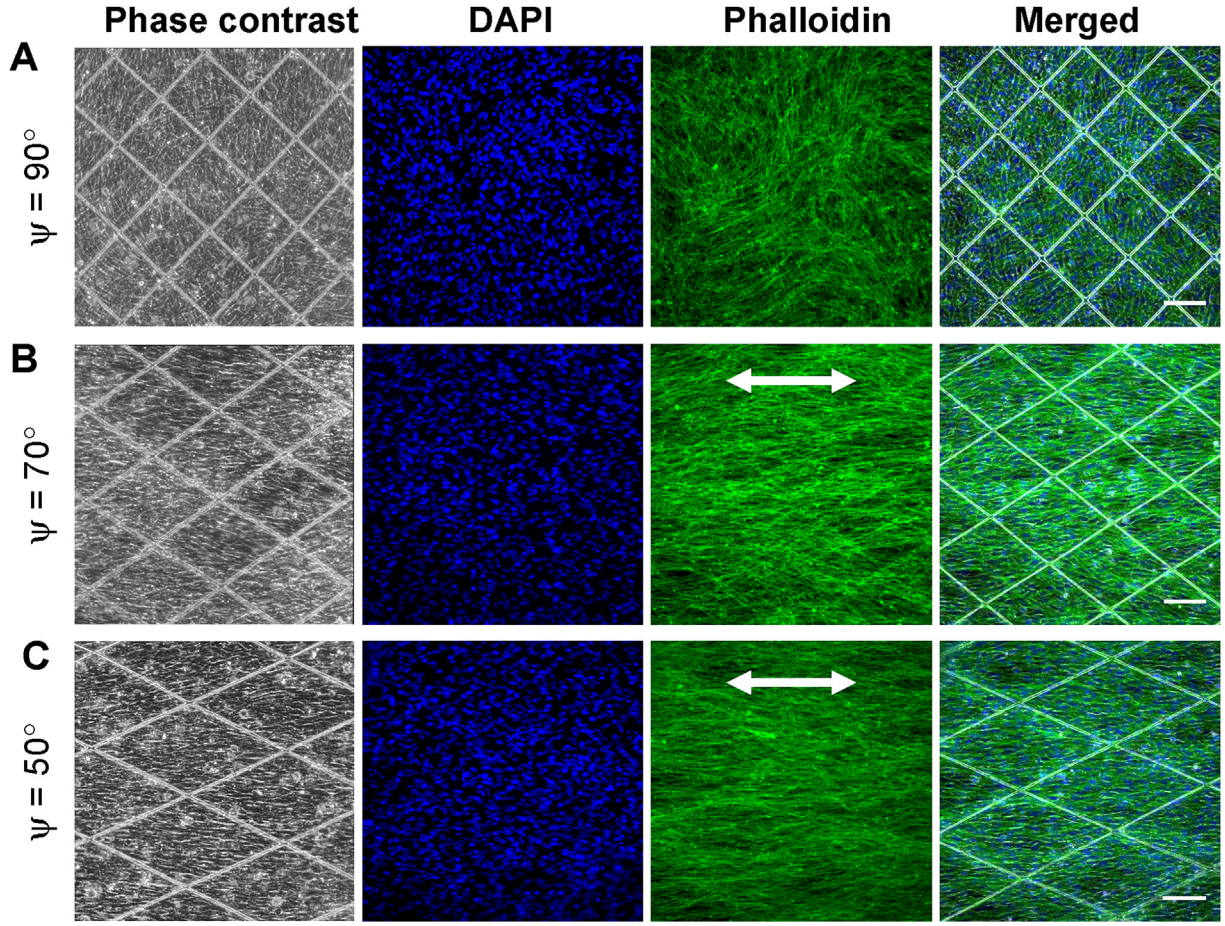


**Fig. 4.** F-actin alignment in self-organized cell sheets generated using micromesh scaffolds with varying mesh shapes. A–C: Comparison of F-actin alignment in C2C12 cell sheets fabricated using micromesh scaffolds with different mesh shapes ($\psi = 90^\circ$, $70^\circ$ and $50^\circ$). Diamond meshes ($\psi = 70^\circ$ and $50^\circ$) exhibited alignment in the major axis, which appeared to be more pronounced with decreasing ψ. White arrows in B and C indicate alignment direction. Scale bar: 100 μm.

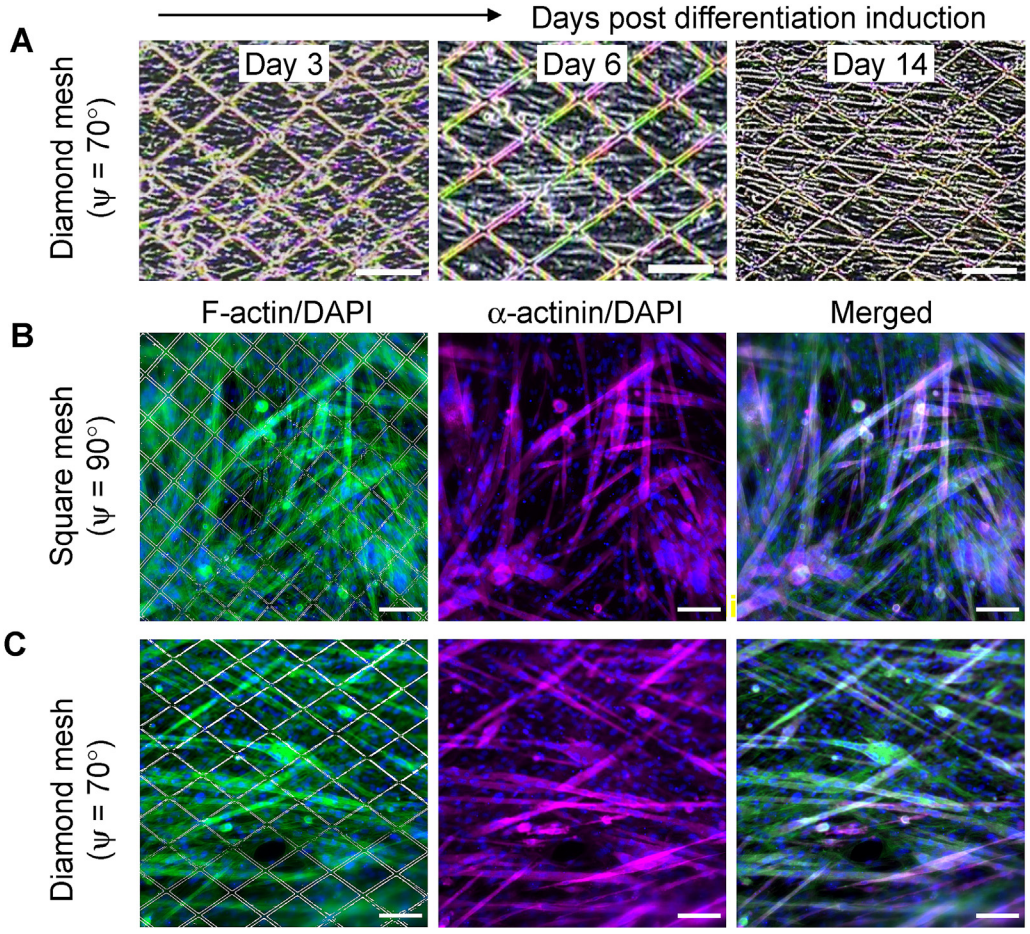


**Fig. 5.** Orientation of myotubes formed by the sheet-forming C2C12 cells following differentiation induction. A: Images depicting myotube formation and alignment on a diamond mesh at different days post differentiation induction. B: Fluorescent images showing randomly oriented myotubes on a square mesh. C: Fluorescent images of aligned myotubes on a diamond mesh. Comparatively, myotubes formed on a diamond mesh appeared to be more aligned than those on a square mesh, with alignment conforming to the major shape axis. Scale bar is 100 μm.

immature at Day 14, the time when fixation was performed. Remarkably, myotubes formed on mesh were morphologically similar to those derived from dish-cultured C2C12, and, as expected, the orientation of myotubes on dish was random, unlike on the diamond mesh (Fig. S5A, B).

Taken together, the results demonstrate that the global alignment property induced by the microscale mesh shape could be preserved even after myotube formation, hinting at the possibility of obtaining orientated myotube sheets from the aligned C2C12 cell sheets.

## 4. Discussions

Cell alignment is critical to various cell functions both in vivo and in vitro, including cytoskeleton reorganization, membrane protein relocation, nucleus gene expression, and ECM remodeling [29]. For instance, spatial orientation of cells contributes to pattern formation during embryogenesis [29], and plays critical roles in the maturation of neurons [30]. In vivo tissues, including skeletal muscles and cardiac tissues, display characteristic straited morphology owing to the unidirectional alignment of their cells. This property is important for coordinated generation of contractile forces by these tissues. Hence, alignment is an important consideration when fabricating cell sheets for application in the regeneration of such orientated tissues.

In this study, we have demonstrated macroscale control of cell alignment in self-organized C2C12 cell sheets by tuning the microscale geometry of 2D microstructured mesh scaffolds. By designing micromesh scaffolds with diamond shapes of varying acuteness (achieved by changing the shape angle from $\psi = 90°$~$50°$, for $L = 200$ μm), we have found that alignment intensity increased with increasing acuteness of the diamond shape (Fig. 3C), implying that cell alignment on the 2D micromesh scaffolds could be sensitive to mesh shape anisotropy. This alignment response demonstrates that C2C12 cells could sense and respond to geometrical cues provided by the scaffold microstructure, which define their adhesion microenvironment. Indeed, cells are known to sense their mechanical environment through cell-substrate and cell-cell adhesion, and to respond to the geometrical as well as physical boundary conditions [31]. Adhesion proteins such as integrins and cadherins on the cell exterior are known to sense the physical adhesion microenvironment and to mediate a mechanoresponse via the actin cytoskeleton such that cells are able to respond to both geometrical and mechanical cues in their adhesion microenvironment [32,33].

In a past study using human dermal fibroblasts, Costa et al. [34] found that cells aligned parallel to free edges in partially constrained thin gels, but randomly and independently of geometry in fully constrained gel. Based on their findings, they proposed that rather than align along the local direction of greatest tension, cells

orient parallel to the local free boundary [34]. More recently, using an in vitro collagen matrix system that exerts a uniaxially-fixed mechanical boundary condition, Kim et al. demonstrated that mouse osteoblast-like MC3T3-E1 cells could be evoked to align along the uniaxial boundary condition [35]. These studies have demonstrated cell alignment as a mechanoresponse dictated by the macroscale mechanical conditions of the culture substrate. In the same context, and in light of the fact that the microstructure (mesh shape) defines the global mechanical property (mechanical isotropic or anisotropic) of the micromesh scaffolds, the increase in alignment intensity with acuteness of the diamond meshes may be interpreted as evidence of cells sensing the global mechanical anisotropy that results from the microscale geometry of the scaffold microstructure.

While support for 3D scaffolds and culture systems has grown steadily over recent years [36,37], especially for cancer and other studies which require mimicking the in-vivo microenvironment for more accurate results [38], in tissue engineering, 2D culture systems remain a platform of choice for mass cell culture because they are generally low cost, easy to image, relatively easy to design to control cell behavior, among other advantages. For cell sheets, which are themselves 2D cellular constructs, 2D scaffolds and culture systems are more compatible and offers a higher degree of controllability. Indeed, we have not only succeeded in demonstrating that the 2D micromesh scaffolds can induce self-organized cell sheet formation mediated by cell-cell adhesion, but also shown that by modulating the mesh shape (pore shape), we can control macroscale alignment as a cellular response to the scaffold microstructure. It is worth mentioning that our culture system employing the 2D micromesh scaffolds is a hybrid of 2D and 3D culture systems in the sense that the adhesion restriction to which cells are exposed entices them to undergo self-organization while relying majorly on cell-cell interaction, as would occur in 3D culture systems.

Furthermore, our approach offers additional advantages compared with existing methods that hitherto have been used to induce cell alignment in cell sheets, such as microcontact printing [39] and mechanical stretch [18,40]. As demonstrated in this study, alignment on the 2D micromesh scaffolds emerges from the cell-material interaction as a natural response to the scaffold microstructure. In other words, this provides an approach to control cell alignment in cell sheets without the need to apply mechanical stretch to the fragile sheets, or perform complex micropatterning procedures. Moreover, the mesh scaffolds help to contribute to the mechanical strength of the cell sheets, which makes handling easier. Nevertheless, one notable limitation of our approach is that to some extent, alignment depends on cell type, with cells of mesenchymal origin, such as C2C12 cells and TIG-120 (Fig. S4) showing better alignment performance compared with epithelial cells. Remarkably, the latter did not yield notable alignment even on the diamond meshes (data not shown). We postulate that mesenchymal cells may perform better on the micromesh scaffold due to their polarized spindle-like shape and strongly adherent property.

Mechanistically, the emergence of alignment on suspended scaffolds under restricted adhesion condition provides a novel platform to investigate alignment as a mechanoresponse mediated by cell-cell adhesion, in addition to the widely investigated cell-substrate adhesion [40–42]. This aspect remains to be explored further in our future studies.

## 5. Conclusion

In the present study, we aimed to clarify the influence of scaffold microstructure on macroscale cell alignment in self-organized cell sheets generated using adhesion-limiting micromesh scaffolds. We found that whereas diamond meshes produced cell sheets with a characteristic uniaxial alignment in the direction of the major shape axis, square meshes on the other hand yielded cell sheets with random orientation, demonstrating that the shape of the scaffold microstructure exerts considerable influence on cell alignment. Moreover, alignment intensity on the diamond meshes was found to increase concomitantly with the acuteness of the diamond shape, implying sensitivity to mesh shape anisotropy. We further confirmed that myotubes derived from aligned C2C12 cells could also exhibit similar alignment. Collectively, our results demonstrate that tuning the microscale geometry of a scaffold can induce macroscale cell alignment in self-organized cell sheets. Insights from this study would be relevant to the design of instructive scaffolds for generating aligned cell sheets with potential application in the regeneration of aligned tissues, including cardiac tissues, skeletal muscles, tendons, and ligaments. Future work will explore the molecular mechanisms underlying the geometry mechanosensing exhibited by C2C12 cells in this study.

## Credit author statement

K.O.O. conceived and designed experiments, and wrote the manuscript; Y.K. performed experiments and analyzed experimental data; T.A., discussed, reviewed, and edited the manuscript. All authors discussed and interpreted results and commented on the manuscript.

## Declaration of competing interest

All the authors have no conflict of interest to declare.

## Acknowledgement

This research was supported by AMED PRIME under Grant Number 20gm5810023h0004, JSPS KAKENHI Grant Number JP20H02594, and partially by the Cooperative Research Program (Joint Usage/Research Center program) of Institute for Frontier Life and Medical Sciences, Kyoto University. We are thankful to lab members, Yuta Ando, Junko Sunaga, Yoshitaka Kameo and Koichiro Maki for useful discussions. We are grateful to the staff of Kyoto University Nano Technology Hub in “Nanotechnology Platform Project” for technical support with the fabrication of the micromesh scaffolds used in this study.

## Appendix A. Supplementary data

Supplementary data to this article can be found online at https://doi.org/10.1016/j.mtadv.2021.100194.

## References

[1] M. Kawamura, S. Miyagawa, K. Miki, A. Saito, S. Fukushima, T. Higuchi, T. Kawamura, T. Kuratani, T. Daimon, T. Shimizu, T. Okano, Y. Sawa, Feasibility, safety, and therapeutic efficacy of human induced pluripotent stem cell-derived cardiomyocyte sheets in a porcine ischemic cardiomyopathy model, Circulation 126 (11_suppl_1) (2012) S29–S37.
[2] S. Masuda, T. Shimizu, M. Yamato, T. Okano, Cell sheet engineering for heart tissue repair, Adv. Drug Deliv. Rev. 60 (2) (2008) 277–285.
[3] B. Venugopal, S.J. Shenoy, S. Mohan, P.R. Anil Kumar, T.V. Kumary, Bioengineered corneal epithelial cell sheet from mesenchymal stem cells—a functional alternative to limbal stem cells for ocular surface reconstruction, J. Biomed. Mater. Res. B Appl. Biomater. 108 (3) (2020) 1033–1045.
[4] K. Nishida, M. Yamato, Y. Hayashida, K. Watanabe, K. Yamamoto, E. Adachi, S. Nagai, A. Kikuchi, N. Maeda, H. Watanabe, T. Okano, Y. Tano, Corneal reconstruction with tissue-engineered cell sheets composed of autologous oral mucosal epithelium, N. Engl. J. Med. 351 (12) (2004) 1187–1196.
[5] H. Thorp, K. Kim, M. Kondo, T. Maak, D.W. Grainger, T. Okano, Trends in articular cartilage tissue engineering: 3D mesenchymal stem cell sheets as

candidates for engineered hyaline-like cartilage, Cells 10 (3) (2021) 643.
[6] H. Sekine, T. Shimizu, I. Dobashi, K. Matsuura, N. Hagiwara, M. Takahashi, E. Kobayashi, M. Yamato, T. Okano, Cardiac cell sheet transplantation improves damaged heart function via superior cell survival in comparison with dissociated cell injection, Tissue Eng. 17 (23–24) (2011) 2973–2980.
[7] S. Miyagawa, Y. Sawa, Building a new strategy for treating heart failure using Induced Pluripotent Stem Cells, J. Cardiol. 72 (6) (2018) 445–448.
[8] A. Valentín, J.D. Humphrey, Modeling effects of axial extension on arterial growth and remodeling, Med. Biol. Eng. Comput. 47 (9) (2009) 979–987.
[9] J. Yang, M. Yamato, C. Kohno, A. Nishimoto, H. Sekine, F. Fukai, T. Okano, Cell sheet engineering: recreating tissues without biodegradable scaffolds, Biomaterials 26 (33) (2005) 6415–6422.
[10] J. Kobayashi, A. Kikuchi, T. Aoyagi, T. Okano, Cell sheet tissue engineering: cell sheet preparation, harvesting/manipulation, and transplantation, J. Biomed. Mater. Res. 107 (5) (2019) 955–967.
[11] J. Meyle, K. Gültig, M. Brich, H. Hämmerle, W. Nisch, Contact guidance of fibroblasts on biomaterial surfaces, J. Mater. Sci. Mater. Med. 5 (6) (1994) 463–466.
[12] C.H. Lee, H.J. Shin, I.H. Cho, Y.-M. Kang, I.A. Kim, K.-D. Park, J.-W. Shin, Nanofiber alignment and direction of mechanical strain affect the ECM production of human ACL fibroblast, Biomaterials 26 (11) (2005) 1261–1270.
[13] B. Zhu, Q. Lu, J. Yin, J. Hu, Z. Wang, Alignment of osteoblast-like cells and cell-produced collagen matrix induced by nanogrooves, Tissue Eng. 11 (5–6) (2005) 825–834.
[14] S.Y. Chew, R. Mi, A. Hoke, K.W. Leong, Aligned protein–polymer composite fibers enhance nerve regeneration: a potential tissue-engineering platform, Adv. Funct. Mater. 17 (8) (2007) 1288–1296.
[15] H. Takahashi, M. Nakayama, K. Itoga, M. Yamato, T. Okano, Micropatterned thermoresponsive polymer brush surfaces for fabricating cell sheets with well-controlled orientational structures, Biomacromolecules 12 (5) (2011) 1414–1418.
[16] H. Takahashi, T. Shimizu, M. Nakayama, M. Yamato, T. Okano, The use of anisotropic cell sheets to control orientation during the self-organization of 3D muscle tissue, Biomaterials 34 (30) (2013) 7372–7380.
[17] G. Grenier, M. Rémy-Zolghadri, D. Larouche, R. Gauvin, K. Baker, F. Bergeron, D. Dupuis, E. Langelier, D. Rancourt, F.A. Auger, L. Germain, Tissue reorganization in response to mechanical load increases functionality, Tissue Eng. 11 (1–2) (2005) 90–100.
[18] J. Homma, S. Shimizu, H. Sekine, K. Matsuura, T. Shimizu, A novel method to align cells in a cardiac tissue-like construct fabricated by cell sheet-based tissue engineering, J. Tissue Eng. Reg. Med. 14 (7) (2020) 944–954.
[19] A. Ovsianikov, A. Khademhosseini, V. Mironov, The synergy of scaffold-based and scaffold-free tissue engineering strategies, Trends Biotechnol. 36 (4) (2018) 348–357.
[20] K.O. Okeyo, O. Kurosawa, H. Oana, H. Kotera, M. Washizu, Minimization of cell-substrate interaction using suspended microstructured meshes initiates cell sheet formation by self-assembly organization, Biomed. Phy. Eng. Express 2 (6) (2016), 065019.
[21] K.O. Okeyo, O. Kurosawa, S. Yamazaki, H. Oana, H. Kotera, H. Nakauchi, M. Washizu, Cell adhesion minimization by a novel mesh culture method mechanically directs trophoblast differentiation and self-assembly organization of human pluripotent stem cells, Tissue Eng. C Methods 21 (10) (2015) 1105–1115.
[22] Y. Ando, K.O. Okeyo, T. Adachi, Modulation of adhesion microenvironment using mesh substrates triggers self-organization and primordial germ cell-like differentiation in mouse ES cells, APL Bioengineering 3 (1) (2019), 016102.
[23] R. Yanaru, K.O. Okeyo, O. Kurosawa, H. Oana, H. Kotera, M. Washizu, Control of cell orientation in mesenchymal cell sheets fabricated using microstructured mesh sheet, in: 2014 International Symposium on Micro-NanoMechatronics and Human Science (MHS), 2014, pp. 1–5.
[24] T. Asano, T. Ishizua, H. Yawo, Optically controlled contraction of photosensitive skeletal muscle cells, Biotechnol. Bioeng. 109 (1) (2012) 199–204.
[25] Z. Püspöki, M. Storath, D. Sage, M. Unser, Transforms and operators for directional bioimage analysis: a survey, Adv. Anat. Embryol. Cell Biol. 219 (2016) 69–93.
[26] A. Brugués, E. Anon, V. Conte, J.H. Veldhuis, M. Gupta, J. Colombelli, J.J. Muñoz, G.W. Brodland, B. Ladoux, X. Trepat, Forces driving epithelial wound healing, Nat. Phys. 10 (9) (2014) 683–690.
[27] A.B.C. Buskermolen, T. Ristori, D. Mostert, M.C. van Turnhout, S.S. Shishvan, S. Loerakker, N.A. Kurniawan, V.S. Deshpande, C.V.C. Bouten, Cellular contact guidance emerges from gap avoidance, Cell Rep Phys Sci 1 (5) (2020), 100055-100055.
[28] A.B.C. Buskermolen, H. Suresh, S.S. Shishvan, A. Vigliotti, A. DeSimone, N.A. Kurniawan, C.V.C. Bouten, V.S. Deshpande, Entropic forces drive cellular contact guidance, Biophys. J. 116 (10) (2019) 1994–2008.
[29] Y. Li, G. Huang, X. Zhang, L. Wang, Y. Du, T.J. Lu, F. Xu, Engineering cell alignment in vitro, Biotechnol. Adv. 32 (2) (2014) 347–365.
[30] S.Y. Chew, R. Mi, A. Hoke, K.W. Leong, The effect of the alignment of electrospun fibrous scaffolds on Schwann cell maturation, Biomaterials 29 (6) (2008) 653–661.
[31] M. Werner, N.A. Kurniawan, C.V.C. Bouten, Cellular geometry sensing at different length scales and its implications for scaffold design, Materials 13 (4) (2020) 963.
[32] A. Haupt, N. Minc, How cells sense their own shape – mechanisms to probe cell geometry and their implications in cellular organization and function, J. Cell Sci. 131 (6) (2018) jcs214015.
[33] M. Murrell, P.W. Oakes, M. Lenz, M.L. Gardel, Forcing cells into shape: the mechanics of actomyosin contractility, Nat. Rev. Mol. Cell Biol. 16 (8) (2015) 486–498.
[34] K.D. Costa, E.J. Lee, J.W. Holmes, Creating alignment and anisotropy in engineered heart tissue: role of boundary conditions in a model three-dimensional culture system, Tissue Eng. 9 (4) (2003) 567–577.
[35] J. Kim, K. Ishikawa, J. Sunaga, T. Adachi, Uniaxially fixed mechanical boundary condition elicits cellular alignment in collagen matrix with induction of osteogenesis, Sci. Rep. 11 (1) (2021) 9009.
[36] M. Ravi, V. Paramesh, S.R. Kaviya, E. Anuradha, F.D.P. Solomon, 3D cell culture systems: advantages and applications, J. Cell. Physiol. 230 (1) (2015) 16–26.
[37] F. Pampaloni, E.G. Reynaud, E.H.K. Stelzer, The third dimension bridges the gap between cell culture and live tissue, Nat. Rev. Mol. Cell Biol. 8 (10) (2007) 839–845.
[38] M. Kapałczyńska, T. Kolenda, W. Przybyła, M. Zajączkowska, A. Teresiak, V. Filas, M. Ibbs, R. Bliźniak, Ł. Łuczewski, K. Lamperska, 2D and 3D cell cultures - a comparison of different types of cancer cell cultures, Arch. Med. Sci. 14 (4) (2018) 910–919.
[39] C. Williams, Y. Tsuda, B.C. Isenberg, M. Yamato, T. Shimizu, T. Okano, J.Y. Wong, Aligned cell sheets grown on thermo-responsive substrates with microcontact printed protein patterns, Adv. Mater. 21 (21) (2009) 2161–2164.
[40] S.J. Kim, H.R. Cho, K.W. Cho, S. Qiao, J.S. Rhim, M. Soh, T. Kim, M.K. Choi, C. Choi, I. Park, N.S. Hwang, T. Hyeon, S.H. Choi, N. Lu, D.-H. Kim, Multifunctional cell-culture platform for aligned cell sheet monitoring, transfer printing, and therapy, ACS Nano 9 (3) (2015) 2677–2688.
[41] R.J. Petrie, A.D. Doyle, K.M. Yamada, Random versus directionally persistent cell migration, Nat. Rev. Mol. Cell Biol. 10 (8) (2009) 538–549.
[42] K. Chen, A. Vigliotti, M. Bacca, R.M. McMeeking, V.S. Deshpande, J.W. Holmes, Role of boundary conditions in determining cell alignment in response to stretch, Proc. Natl. Acad. Sci. Unit. States Am. 115 (5) (2018) 986–991.